Assessing Heterogeneity in Soil Nitrogen Cycling: A Plot-Scale Approach

Peter Baas*
Jacqueline E. Mohan
Odum School of Ecology
Univ. of Georgia
140 E. Green St.
Athens, GA 30602

Daniel Markewitz
Warnell School of Forestry and Natural
  Resources
Univ. of Georgia
180 E. Green St.
Athens, GA 30602

Jennifer D. Knoepp
U.S. Forest Service
Southern Research Station
Coweeta Hydrologic Lab.
3160 Coweeta Lab Road
Otto, NC 28763

The high level of spatial and temporal heterogeneity in soil N cycling processes hinders our ability to develop an ecosystem-wide understanding of this cycle. This study examined how incorporating an intensive assessment of spatial variability for soil moisture, C, nutrients, and soil texture can better explain ecosystem N cycling at the plot scale. Five sites distributed across a regionally representative vegetation and elevation gradient at the Coweeta Hydrologic Laboratory in the southern Appalachian Mountains were sampled five times between November 2010 and March 2012. We used electromagnetic induction (EMI) to survey for soil moisture, soil texture, and near-infrared reflectance spectroscopy (NIRS) to estimate extractable NH_4^+, total C, and total N concentrations. Laboratory assays of nitrification and denitrification potential rates were used as an index for N cycling dynamics. Multivariate regression analysis indicated that the NIRS and EMI survey data explained 30 to 90% of the variability in potential nitrification rates ($p < 0.01$) and 16 to 70% of variability in potential denitrification rates ($p < 0.01$). Two extrapolation approaches were used to calculate the mean and the variability of potential rates: (i) stratified selection of collected samples based on EMI and NIRS predictors; and (ii) random selection of collected samples. The mean for potential nitrification rates based on EMI and NIRS stratification yielded similar (oak–pine and mixed oak) and greater (northern hardwood and cove hardwood) rates, whereas potential denitrification rates were greater in all sites for the stratified-based estimates. This study demonstrated that the application of geophysical tools may enhance our ecosystem-level understanding of the N cycle.

Abbreviations: CH, cove hardwood; EMI, electromagnetic induction; MO-high, high-elevation mixed oak; MO-low, low-elevation mixed oak; NIRS, near-infrared reflectance spectroscopy; NH, northern hardwood; OP, oak–pine; pDNF, potential denitrification; pNTR, potential nitrification; WS, Watershed.

S oil N cycling processes are heterogeneous in both space and time. Process rates can dramatically change across the range of centimeters to meters and minutes to days, hindering our ability to predict and model these dynamics (Groffman et al., 2009; McClain et al., 2003). The environmental factors (i.e., soil moisture, pH, inorganic N concentrations, organic N, and available C) controlling N cycling processes such as N mineralization (Knoepp et al., 2008; Pastor et al., 1984; Pastor and Post, 1986), nitrification (Breuer et al., 2002; Nielsen and Revsbech, 1998; Sahrawat, 2008; Ste-Marie and Paré, 1999), and denitrification (Burgin et al., 2010; Firestone et al., 1980; Groffman and Tiedje, 1991) are well documented. However, the complexity and heterogeneity of these environmental factors create hotspots and hot moments with accelerated N transformation rates (Burgin et al., 2010; Johnson et al., 2010; Parkin et al., 1987; Schimel and Bennett,

2004) that are challenging to quantify and model (Groffman et al., 2009; McClain et al., 2003).

Hydrologic models in combination with soil biogeochemical models such as the NGAS Century (Parton et al., 1996) simulate N_2 and N_2O emissions from nitrification and denitrification using large watershed scale patterns of soil moisture (Band et al., 2001; Swank and Crossley, 1988; Tague, 2009; Tague et al., 2010) but lack utility at the plot scale ($\sim$ha) (Tague et al., 2010). Approaches capable of capturing fine-scale heterogeneity are needed to improve our ability to model and scale N cycling rates and fluxes (Groffman et al., 2009; Tague et al., 2010).

Geophysical techniques such as electromagnetic induction (EMI) provide a quantitative means to assess fine-scale soil texture and moisture variations through the measurement of soil conductivity (Abdu et al., 2008; Robinson et al., 2008b). Soil conductivity is mainly controlled by volumetric water content, clay content, temperature, and salinity (Everett, 2005; Friedman, 2005). In agricultural and marine systems, research has shown that conductivity is controlled by nutrient concentrations and salinity (Corwin and Lesch, 2005; Sheets et al., 1994; Zhu et al., 2010), whereas in forested systems, soil moisture and soil texture are the controlling factors (Sheets and Hendrickx, 1995; Triantafilis and Lesch, 2005). Therefore, EMI approaches have been used for soil textural (Triantafilis and Lesch, 2005; Weller et al., 2007) and moisture (Reedy and Scanlon, 2003; Robinson et al., 2008b; Sheets and Hendrickx, 1995) assessments but far less commonly to estimate biogeochemical patterns and processes (Cockx et al., 2005). Unlike traditional soil surveys methods, EMI rapidly captures thousands of measurements per hectare. Combining the high-spatial-intensity soil geophysical data from EMI with field-portable spectrophotometric sensors such as near-infrared reflectance spectroscopy (NIRS), which provides soil chemical attributes, allows mapping of both physical and chemical attributes. Both EMI and NIRS map layers have been used extensively in precision agriculture to predict and optimize crop yields (van Vuuren et al., 2006; Zhang et al., 2002).

The southern Appalachian Mountains have been described as the "water tower" of the Southeast (Gragson and Bolstad, 2006), making stream and river water quality important for the regional water supply. Nitrate concentrations in particular increase with anthropogenic disturbance and have been found to be a key player in regional water quality (Knoepp and Clinton, 2009). Nitrate is the mobile form of inorganic N in soils often susceptible to leaching (Aber et al., 1998, 1989). Therefore, this study focused on the process that produces NO_3^- (i.e., nitrification) and the process that removes it from the ecosystem by converting it into a gaseous form (i.e., denitrification), thus preventing leaching. Previous studies have identified soil moisture, NH_4^+ concentrations, C/N ratios, and pH to be the main drivers of nitrification rates (Donaldson and Henderson, 1990; Knoepp and Vose, 2007; Robertson and Vitousek, 1981; Sahrawat, 2008), whereas denitrification rates are generally

thought to be controlled by soil moisture, NO_3^- concentrations, and organic C availability (Groffman, 2012; Tiedje et al., 1984). In addition, wetting and drying cycles have been found to stimulate mineralization, nitrification (Cabrera, 1993; Fierer and Schimel, 2002), and denitrification (Groffman and Tiedje, 1988), making variability in soil moisture an important factor controlling process rates both instantaneous and via distal controls on the community composition (Groffman et al., 1988; Wallenstein et al., 2006).

In this study, we investigated the potential of high-spatial-resolution EMI and NIRS measurements to estimate the variability of potential nitrification (pNTR) and potential denitrification (pDNF) rates in five forest types along a gradient in elevation, vegetation, N, and water availability in the southern Appalachian Mountains.

We hypothesized that patterns of spatial variability in soil conductivity, a proxy for soil moisture, will relate to patterns of process rates for nitrification and denitrification. In addition, we hypothesized that greater total C and inorganic N concentrations would result in higher pDNF rates, whereas pNTR would be positively correlated to inorganic N concentrations. We expected spatial autocorrelation to indicate pNTR to be less heterogeneous (large range) than pDNF (small range) because redox conditions that drive pDNF are probably more variable across plots. We used spatial modeling techniques to predict pNTR and pDNF providing insights concerning where we could expect high and low process rates. This approach could dramatically improve both sample collection efficiency as well as the accuracy of predicted N cycling rates across a larger spatial scale.

METHODS
Study Site

The study was conducted at the Coweeta Hydrologic Laboratory, a 2180-ha U.S. Forest Service experimental forest in the southern Appalachian Mountains in western North Carolina. This area receives an average of 1800 ± 34 (low elevation) to 2400 ± 44 mm (high elevation) of precipitation a year (Coweeta Long-Term Ecological Research, 1934–2011, http://coweeta.uga.edu/dbpublic/dataset_details.asp?accession=1011). The highest average air temperatures are between June and August (20°C), and the lowest average air temperatures are between December and January (5°C). The growing season starts in May and ends in September (Swift et al., 1988).

We examined five sites (80 by 80 m) that represent the major vegetation types within the Coweeta basin. All five sites are located in reference watersheds that have been undisturbed since 1929 (Knoepp and Swank, 1998). Watershed 18 is a low-elevation watershed (13 ha) and includes xeric oak–pine (OP), cove hardwood (CH), and low-elevation mesic mixed oak (MO-low) forest community types. Watershed 27 is a high-elevation watershed (39 ha) and includes high-elevation mesic mixed oak (MO-high) and northern hardwood (NH) forest community types. Table 1 provides detailed information regarding the elevation, slope, dominant vegetation, and soils for each site.

Table 1. Selected site characteristics. Data were compiled from Coweeta Long-Term Ecological Research Program records (see www.coweeta.uga.edu for additional information). Modified from Knoepp and Swank (1998). Soils data were determined on soil profiles extending from surface to parent material (Thomas, 1996).

Parameter	Oak–pine	Cove hardwood	Low-elevation mixed oak	High-elevation mixed oak	Northern hardwood
Location	83°26′ N 35°3′ W	83°26′ N 35°2′ W	83°26′ N 35°2′ W	83°27′ N 35°2′ W	83°27′ N 35°1′ W
Elevation, m	788	801	860	1094	1389
Aspect, °	180	340	15	75	20
Slope, °	34	21	34	33	33
Vegetation	oak–pine	cove hardwood	mixed oak	mixed oak	northern hardwoods
Dominant species	*Pinus rigida* Mill. *Quercus coccinea* Münchh. *Quercus prinus* Willd. *Carya* spp. *Kalmia latifolia* L.	*Liriodendron tulipifera* L. *Quercus prinus* *Carya* spp.	*Quercus prinus* *Carya* spp. *Quercus rubra* L. *Rhododendron maximum* L.	*Quercus prinus* *Quercus rubra* *Carya* spp. *Rhododendron maximum*	*Betula alleghaniensis* Britton *Quercus rubra* *Betula lenta* L. *Tilia heterophylla* Vent.
Moisture regime	xeric	mesic	mesic	mesic	mesic
Soil series	Evard–Cowee Chandler Edneyville–Chestnut	Saunook Tuckaseegee	Trimont	Chandler	Plott
Soil textures	fine-loamy coarse-loamy coarse-loamy	fine-loamy fine-loamy	fine-loamy	coarse-loamy	coarse-loamy
Soil subgroups	Typic Hapludults Typic Dystrochrepts	Humic Hapludults Typic Dystrochrepts	Humic Hapludults	Typic Dystrochrept	Typic Haplumbrepts

Soil Sampling and Incubations

We determined potential nitrification (pNTR) and potential denitrification (pDNF) on fresh soil samples collected in March 2011, July 2011, November 2011, and March 2012. Using a stainless steel soil push tube, cores (15 cm mineral soil) were collected from randomly selected locations (three to six) within each of the five sites (OP, CH, MO-low, MO-high, and NH). For potential nitrification, $n_{total} = 67$ ($n_{OP} = 12$, $n_{CH} = 16$, $n_{MO\text{-low}} = 16$, $n_{MO\text{-high}} = 7$, $n_{NH} = 16$), and for potential denitrification, $n_{total} = 87$ ($n_{OP} = 15$, $n_{CH} = 17$, $n_{MO\text{-low}} = 16$, $n_{MO\text{-high}} = 20$, $n_{NH} = 19$). The location of each sample was obtained using an Archer GPS (Juniper Systems Inc.). We divided core samples into forest floor and 0- to 15-cm-depth mineral soil (pNTR) or forest floor and 0- to 5-, 5- to 10-, and 10- to 15-cm-depth mineral soil (pDNF), and stored the samples in reclosable plastic bags at 4°C. Each soil sample was sieved (<2 mm) and homogenized. Gravimetric soil moisture was determined by oven drying a 10-g subsample of each soil at 105°C to constant weight. Potential nitrification assays were determined on field-moist soils within 72 h of collection, and pDNF assays were conducted on field-moist soils stored at 4°C for <2 wk.

We used the amended slurry incubation method for pNTR determinations on both soil and forest floor ($n_{total} = 67$) samples (Bodelier et al., 1996). Five-gram samples of sieved soil or forest floor were placed in 37-mL serum vials with 15 mL of media [0.33 g L^{-1} (NH$_4$)$_2$SO$_4$ in deionized (DI) water buffered with 0.14 g L^{-1} K$_2$HPO$_4$ and 0.027 g L^{-1} KH$_2$PO$_4$) (pH = 7.5). Each vial was wrapped in Al foil, with an Al foil cap to prevent evaporation and UV light inhibition of NH$_3$ oxidizers. After the addition of the media, the vials were shaken at 10 relative centrifugal force (rcf) at 25°C; 2-mL subsamples were collected after 0.5, 2, 6 to 8, and 24 h of incubation using a cut-off pipette tip. Subsamples were centrifuged for 10 min at 11,000 rcf and the supernatant was immediately frozen at −20°C until analysis for NO$_2^-$ + NO$_3^-$ using colorimetric methods (Bendschneider and Robinson, 1952).

Potential denitrification rates were determined using the acetylene block method (Groffman et al., 1999) on both soil and forest floor samples ($n_{total} = 87$). Five-gram samples of sieved soil (2 g for forest floor samples) were added to 37-mL serum vials. The serum vials were purged with He for 1 min to displace O$_2$ from the vial, and then 5 mL of incubation media was added to the serum vials. The media consisted of dextrose (1 mmol L^{-1}) and NaNO$_3$ (1 mmol L^{-1}) in DI water purged for 30 min with He gas. Assays were initiated by replacing 4 mL of headspace with 99% pure acetylene (10% v/v). The samples were incubated at 20°C while shaking (5 rcf) for 6 h. Gas subsamples were taken 0.5, 2, and 6 h after initiation of the incubation and stored in 3-mL gas vials until analysis for N$_2$O on a gas chromatograph with electron capture detector (Shimadzu Corporation GC-14A) with a 10-port Valco valve (Valco Instruments) to prevent acetylene from saturating the detector.

Rates of pNTR and pDNF were determined via regression analysis of changes in solution NO$_3^-$ or N$_2$O concentrations with time (rates were accepted if $r^2 > 0.8$). All rate data were calculated per kilogram of dry soil (as µg N kg^{-1} soil h^{-1}). Using the total weight of dry soil or forest floor from each core subsection, a rate was calculated for the whole 0- to 15-cm-depth core (µg N kg^{-1} soil h^{-1}).

In June 2011, georeferenced soil texture analyses were done on each of the five sites (OP, CH, MO-low, MO-high,

and NH) (n = 10 per site) on 0- to 20-cm-depth soil samples collected from randomly distributed locations throughout each 80- by 80-m site. The sample location was also determined using an Archer GPS. Soil texture analysis was done using the hydrometer method (Robertson et al., 1999). In short, soils were oven dried at 105°C to a constant weight and sieved to <2 mm; all roots and rocks were removed and weighed. Forty grams of sieved soil was added to 175-mL plastic bottles with 100 mL of 5% hexametaphosphate and shaken overnight. The next day, the solution was washed through a 53-μm sieve with DI water. The particles captured on the sieve were collected and oven dried (105°C) overnight (this constituted the sand fraction). The suspension that passed through the sieve was placed in a 1-L volumetric cylinder filled to 1 L. The suspension was stirred and a few drops of amyl alcohol was used to reduce foaming. Hydrometer readings were taken at 1.5 and 24 h. Silt and clay fractions were calculated according to Robertson et al. (1999).

Surveying

The EMI surveys were conducted in November 2010, March 2011, July 2011, November 2011, and March 2012. The EMI measurements were collected for 1 h per site, yielding approximately 500 measurements. We used a DUALEM-2S EMI sensor carried at a height of 1 m above the ground connected to an Archer GPS datalogger. The EMI recorded bulk soil conductivity (ECa) for both the horizontal coplanar coils (ECa-3m; theoretical cumulative signal of 70% at 3-m depth) and the perpendicular coils (ECa-1m; theoretical cumulative signal of 70% at 1-m depth), resulting in two measurements per sample location (Beamish, 2011). Temperature varies widely among sites and between seasons and has a significant effect on conductivity readings. Therefore, all EMI conductivity measurements were standardized to the equivalent value at 25°C (EC25) (Reedy and Scanlon, 2003). Spatial analysis of EMI data was done using ArcGIS 10.0. In each site, predicted conductivity measurements were produced by ordinary kriging (Isaaks and Srivastava, 1989; Johnston et al., 2001). Subsequently, predicted values were extracted at soil sampling locations of process rates or soil texture outlined above. For every pixel (∼1 m^2) of the kriged maps, the standard error (SE), lowest value (low), highest value (high), and the Δ (i.e., maximum minus minimum) was calculated across all sampling dates (i.e., ECa-1m-low, ECa-1m-high, ECa-3m-low, ECa-3m-high, SE ECa-1m, SE ECa-3m, ΔECa-1m, and ΔECa-3m). Data were checked for normality using normal Q–Q plots. Ordinary kriging can accommodate non-normal distributions as long as the spatial autocorrelation structure is not masked by extreme values (Isaaks and Srivastava, 1989). Therefore, in the case of non-normal distribution after natural logarithm transformation, the data were checked for extreme value outliers, and points were removed if necessary before kriging analysis.

We used an ASD FieldSpec 3 NIRS (Analytical Spectral Devices Inc.) to assess total soil C and N (Chang and Laird,

2002) and KCl-extractable NH_4^+ (Janik et al., 1998). We used the FieldSpec NIRS, which provides reflectance data with 1-nm resolution between 350- and 2500-nm wavelengths. All NIRS data were first transformed to the first derivative before analysis. For calibration purposes, 46 sieved (<2-mm) oven-dried catalog samples previously analyzed for total C and N with an Elementar Flash EA 1112 NC analyzer (Thermo Scientific) were used. Carbon and N contents were converted to an aerial measure (kg C m^{-2} and g N m^{-2}, respectively) using bulk density measures determined on each of the collected core sections (g cm^{-3}) (n_{total} = 79). Calibration between NIRS and KCl-extractable NH_4^+ was established on the March 2011 and 2012 samples. Twenty-five percent (n = 12 for each sampling time) of the samples collected on those dates were immediately extracted with 2 mol L^{-1} KCl on all mineral soil depths (0–5, 5–10, and 10–15 cm); supernatant NH_4^+ concentrations were analyzed according to colorimetric methods using an Alpkem 3000 Series autoanalyzer (OI Analytical). Calibration models were developed by running full factorial cross-validation multivariate analyses using the Unscrambler software (CAMO Software Inc.) and produced predicted values for total C, total N, and NH_4^+ concentrations.

Model Development and Statistical Analyses

Model development took place in three steps. First, a model was developed to assess correlations between soil physical properties (soil moisture and soil texture) and EMI measurements (ECa-1m-low, ECa-1m-high, ECa-3m-low, ECa-3m-high, SE ECa-1m, SE ECa-3m, ΔECa-1m, and ΔECa-3m). To determine significant correlations between the soil physical properties and conductivity data, stepwise multivariate standard least squares regression analysis was utilized, and the best model was selected by using the corrected Akaike's information criterion. We used the same stepwise regression analysis to predict pNTR and pDNF rates based on EMI and NIRS variables (total C, total N, $NH_4^+{}_{0–5cm}$, $NH_4^+{}_{5–10cm}$, $NH_4^+{}_{10–15cm}$). All data were natural logarithm transformed to acquire normal distribution, and regression residuals were evaluated for the absence of heteroscedasticity. Validation was done by randomly separating the data set into calibration (70%) and validation (30%) data sets. Model parameterization was done using only the calibration data set (training data set), whereas the predicted process rates were confirmed using the validation data set by regressing predicted against observed values.

The second step was to extract predicted EMI and NIRS values for each of the sampling locations. The extracted data were natural logarithm transformed and checked for normality using Q–Q plots in ArcGIS. Subsequently, the parameters selected through the stepwise regression analysis described above were used to estimate process rates across the plots by simple ordinary kriging in ArcGIS 10.0 (Johnston et al., 2001), assigning a predicted potential process rate to each pixel. To assess spatial autocorrelation (major range) and spatial structure (nugget/sill ratio) of the predicted potential process rates, the

Table 2. Soil properties by forest type for the coarse fraction, sand fraction, silt fraction, and clay fraction (0–20-cm depth) collected in June 2011. The values for sand, silt, and clay only consider the <2-mm fraction. The C and N data on < 2mm bulk soil were determined using NIRS.

Site†	n	Coarse	Sand	Silt	Clay	C	N
		———————————— g kg^{-1} ————————————				kg C m^{-2}	kg N m^{-2}
OP	10	180 ± 20 ab‡	820 ± 20 a	110 ± 20 c	70 ± 10 c	3.9 ± 0.3 ab	0.22 ± 0.01 b
CH	10	240 ± 20 a	720 ± 20 ab	170 ± 20 b	110 ± 10 bc	4.5 ± 0.3 ab	0.25 ± 0.01 ab
MO-low	10	140 ± 20 bc	700 ± 20 b	170 ± 10 b	130 ± 10 b	4.3 ± 0.3 ab	0.25 ± 0.01 ab
MO-high	10	150 ± 20 bc	680 ± 40 b	170 ± 20 bc	200 ± 10 a	3.3 ± 0.4 b	0.21 ± 0.01 b
NH	10	100 ± 10 c	550 ± 10 c	250 ± 10 a	200 ± 10 a	5.0 ± 0.3 a	0.27 ± 0.01 a

† OP, oak–pine; CH, cove hardwood; MO-low, low-elevation mixed oak; MO-high, high-elevation mixed oak; NH, northern hardwood.
‡ Data followed by different letters are significantly different at $p < 0.05$.

range, sill, nugget, and nugget/sill ratio were determined using a stable semivariogram fit (Isaaks and Srivastava, 1989; Johnston et al., 2001). A maximum lag distance of 75.4 m (two-thirds of the maximum pairwise distance between sampling points) was considered to prevent interpretations across a larger area than the plot size (Webster and Oliver, 2005). Each standard semivariogram was also tested for directionality or anisotropy (Isaaks and Srivastava, 1989). The root mean squared error never decreased by more the 5% when adding anisotropy into the model and, therefore, isotropy was assumed in all models.

The third step was to compare two extrapolation approaches, one based on random sampling and one based on stratified sampling determined by NIRS and EMI layers. First, we determined the mean, SE, and coefficient of variation (CV) of eight randomly selected samples for which potential rates were measured for each site (i.e., OP, CH, MO-low, MO-high, and NH) spanning all sampling times (i.e., March 2011, July 2011, November 2011, and March 2012). Second, for the stratified approach, we determined the quartiles in data distribution for (EMI and NIRS) predicted process rates for each site spanning all sampling times. We then used the predicted process rates to randomly select two actually measured samples from all four strata as determined by the quartile analysis ($n = 8$). Process rates predicted by NH$_4^+$ concentrations were based on only March 2011 and 2012 ($n = 4$, one selection per stratum).

To assess significant differences in soil characteristics and process rates among different sites and watersheds, we conducted one-way ANOVAs combined with Tukey pairwise comparisons ($p < 0.05$ unless specified differently). All data were tested for normality and natural logarithm transformed if

needed to acquire normality. All statistical analyses were conducted in JMP 9.

RESULTS
Soil Conductivity

Soil conductivity estimated with EMI was not significantly different among sites. Significant differences were found among sampling dates for ECa-3m conductivity, with values measured in November 2011 being greater than those from March 2011 ($F_{2,55} = 3.2$, $p = 0.0473$). The ECa-1m conductivity was greatest in March 2012, exceeding both November and March 2011 ($F_{2,54} = 4.9$, $p = 0.055$).

Soil Properties and Electromagnetic Induction

Soil physical properties varied significantly among sites (Table 2). The coarse fraction percentage (>2 mm) was significantly greater at the CH site than all other sites except OP ($F_{4,42} = 10.6$, $p < 0.001$). The sand percentage was greater in OP than all other sites and lowest in NH ($F_{4,42} = 26.0$, $p < 0.001$). The clay percentage was greatest in Watershed (WS) 27 (MO-high and NH) compared with WS 18 (OP, CH, and MO-low) and lowest in OP ($F_{4,42} = 21.6$, $p < 0.001$), whereas the silt percentage was greater in NH than CH or OP ($F_{4,42} = 10.8$, $p < 0.001$).

Conductivity measures at specific dates were unable to predict soil physical properties (soil texture and soil moisture). However, when pooling all data (i.e., ΔECa-3m, SE ECa-1m, and ECa-3m-high), significant correlations were detected. Overall, ΔECa-3m (i.e., maximum minus minimum) conductivity proved to be the best predictor of soil texture (i.e., coarse fraction and clay percentage; Table 3; Fig. 1). Because

Table 3. Coefficients of determination for regressions between soil conductivity and soil particle abundance, determined as the difference between the minimum and maximum values (ΔECa-3m), the standard error (SE ECa-1m), and the highest value measured (ECa-3m-high). The values indicate the r^2 for $p < 0.05$; + and – indicate the direction of the linear relationship. Watershed 18 includes oak–pine, cove hardwood, and low-elevation mixed oak sites. Watershed 27 includes high-elevation mixed oak and northern hardwood sites.

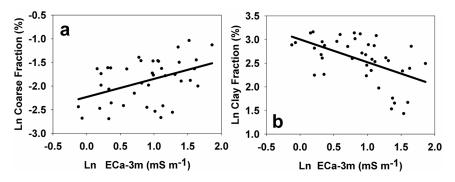|											
		r^2		
Watershed	n	\multicolumn{3}{c}{Sand}		\multicolumn{3}{c}{Silt}		\multicolumn{3}{c}{Clay}
		ΔECa-3m	SE ECa-1m	ECa-3m-high	ΔECa-3m	SE ECa-1m	ECa-3m-high	ΔECa-3m	SE ECa-1m	ECa-3m-high
		g kg^{-1}		
All	50	0.12 (+)	–	–	0.20 (–)	0.12 (–)	–	0.28 (–)	0.20 (–)	–
WS18	30	0.25 (+)	0.45 (+)	–	0.29 (–)	0.53 (–)	–	0.13 (–)†	0.19 (–)	–
WS27	20	–	0.22 (–)†	0.33 (+)	–	0.24 (+)†	0.30 (–)	-	–	–

† Significant at $p < 0.1$.

Fig. 1. Regression between the maximum minus minimum bulk soil conductivity (ΔECa-3m) and (a) coarse soil fraction and (b) clay content for all five sites (0–20-cm depth). Both regression (a) ($p = 0.0055$, $r^2 = 0.19$) and (b) ($p = 0.0004$, $r^2 = 0.28$) were significant.
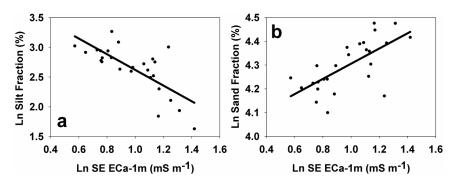

Fig. 2. The (a) silt and (b) sand fractions (0–20-cm depth) regressed with the standard error of the bulk conductivity (SE ECa-1m) for Watershed 18. Both regressions (a) ($p < 0.0001$, $r^2 = 0.53$) and (b) ($p = 0.0003$, $r^2 = 0.45$) were significant.
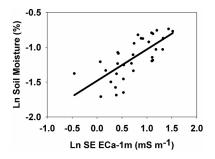

Fig. 3. Fractional soil moisture (0–20-cm depth) regressed against the standard error of the bulk conductivity (SE ECa-1m) for Watershed 27 ($p < 0.0001$, $r^2 = 0.56$).

particle size differed greatly between WS 18 and WS 27 (Table 2), watershed was also a significant predictor in the regression analysis ($p < 0.001$); therefore, the stepwise regression analyses for WS 18 and 27 were conducted separately. No significant relationships were found between pooled conductivity measures and the coarse fraction when separated by watershed. The SE ECa-1m (i.e., standard error of the mean ECa-1m conductivity) was the best predictor for sand and silt contents in WS 18 (Fig. 2), whereas ECa-3m-high (i.e., the highest ECa-3m conductivity for a specific location) was the best predictor of sand and silt contents in WS 27 (Table 3). In WS 27, SE ECa-1m was correlated strongly with soil moisture (Fig. 3). Analysis of data within individual forest types showed that the

best predictor of the soil coarse fraction was ECa-3m-high in OP and MO (second-order polynomial; $r^2 = 0.44$, $p < 0.01$; peak at 1.2 mS and 20% coarse fraction; 95% confidence interval: 0.74–1.67 mS and 14–18% coarse fraction), and CH ($r^2 = 0.81$, $p < 0.001$; 95% confidence interval: 0.51–3.24 mS and 21–29% coarse fraction). No significant correlations with the coarse fraction were found for the NH site.

Nitrogen Cycling and Spatial Data

Calibration models with NIRS were used to predict soil NH_4^+ concentrations and total C and N (Table 4). Potential nitrification was predicted by a multivariate regression model including ECa-3m-high and NIRS-estimated $NH_4^+{}_{5-10cm}$ concentrations (Table 5). For the NH site, the best model included only NIRS-based $NH_4^+{}_{5-10cm}$ concentration (Fig. 4; Table 5). The other four sites were included in a single model, and pNTR was best predicted by ECa-3m-high alone (Table 5). Overall, pDNF rates were best predicted by NIRS-based total C (Table 6). Watershed proved to be a significant predictor in a multivariate regression with SE ECa-1m ($p < 0.0001$); therefore, the analysis was conducted by watershed. The SE ECa-1m proved to have the best predictive power in WS 27 for pDNF rates (Fig. 5; Table 6), while total C provided the best prediction in WS 18 (Table 6).

Spatial autocorrelation of the predicted potential nitrification and denitrification rates as indicated by semivariogram analysis showed that the major range and spatial dependence was often larger than the longest considered distance between points (75.4 m) (Table 7). Major ranges smaller than the plot sizes were found for pNTR (OP, MO-low, and MO-high) and pDNF (all but CH). Spatial structure was strong for all pNTR models (nugget/sill < 0.3), whereas the pDNF models showed weak spatial structure (nugget/sill > 0.3) for WS 18 (OP, CH, and MO-low) and strong spatial structure for WS 27 (MO-high and NH) (Table 7).

Additionally, we compared random to stratified methods (using EMI and NIRS data) of calculating a site-specific mean rate, SE, and CV (Table 8). Comparing the mean rates based on random or stratified selection showed greater estimates with the stratified approach for pNTR in CH ($17 \pm 11\%$) and in NH ($32 \pm 14\%$). No large differences could be observed for pNTR in the OP and MO sites. For pDNF measurements, however, random selection resulted consistently in lower estimates than the stratified approach (OP: $5 \pm 3\%$; CH: $193 \pm 128\%$; MO-low: $14 \pm 3\%$; MO-high: $24 \pm 6\%$; NH: $41 \pm 18\%$). Estimates of SE and CV were generally equal or higher in the stratified approach compared with the random selection approach.

DISCUSSION

The objective of our study was to investigate the utility of high-resolution geophysical methods, which estimate soil water content and soil texture, in assessing plot-scale N cycling heterogeneity in southern Appalachian forests. Our results indicate that a combination of NIRS and EMI techniques are capable of predicting a significant portion of the within- and between-site variability in pNTR and pDNF activity. Soil type (i.e., soil particle size distribution) had a profound effect on the relationships found between process rates and predictive variables (e.g., conductivity, NH_4^+, C).

To understand the mechanisms behind the relationship between soil conductivity and pNTR and pDNF, we first needed to disentangle the relationship between soil conductivity and soil abiotic properties. Soil conductivity is simultaneously controlled by multiple factors, including soil moisture, soil texture, and soil ionic concentrations (Everett, 2005). We found that the abiotic factors controlling soil conductivity were highly watershed dependent. Soil texture alone correlated strongly with conductivity in WS 18 (SE ECa-3m), whereas in WS 27 soil moisture and texture were best correlated to SE ECa-1m and ECa-3m-high, respectively. Although relationships between conductivity and abiotic factors such as soil moisture and texture have been confirmed in studies of agricultural systems (Hedley et al., 2004; Robinson et al., 2008a; Zhu et al., 2010) and managed forest ecosystems (Doolittle et al., 1994; Huth and Poulton, 2007; McBride et al., 1990), rarely are they assessed in soils as heterogeneous as mountain forest soils (Zhu and Lin, 2010). For example, clay content was found to correlate with conductivity measures in a semiarid rangeland ecosystem (Abdu et al., 2008), but no such relationship was found in heterogeneous mountain ecosystems (Zhu et al., 2010). Zhu et al. (2010) suggested that the presence of higher clay content soils on dry slopes confounded the clay–conductivity correlation, which could potentially be the case in our study as well.

Table 4. The *P* values and coefficients of determination for calibration models between near-infrared reflectance spectra (NIRS) and soil C and N contents and extractable NH_4^+. Calibration models were developed on mineral soil (0–15-cm depth) for soil C and N and on both mineral soil and forest floor for NH_4^+. The validation statistics are representative of a regression analysis between observed and predicted values.

Parameter	Entire data set			Calibration data set			Validation data set		
	p	r^2	n	p	r^2	n	p	r^2	n
C content, mineral soil, g kg^{-1}	<0.001	0.997	46	<0.001	0.90	30	0.003	0.65	16
N content, mineral soil, g kg^{-1}	<0.001	0.998	46	<0.001	0.89	30	0.024	0.52	16
Extractable NH_4^+, mg N kg^{-1}	<0.001	0.99	24	†	†	†	†	†	†

† Data set was too small to separate into calibration and validation models.

Table 5. Regression analyses for potential nitrification; + or − indicates the direction of the relationship; *n* is the total number of values used in the model ($NH_4^+$$_{5–10cm}$ for March 2011 and 2012 only and four missing values for SE ECa-3m). The validation statistics are representative of a regression analysis between observed and predicted values.

Site†	Entire data set			Calibration data set			Validation data set			Parameters‡
	RMSE	r^2	n	RMSE	r^2	n	RMSE	r^2	n	
All sites	0.16	0.31**	31	–	–	24	–	–	9	High ECa-3m (−) $NH_4^+$$_{5–10cm}$ (+)
OP, CH, MO	0.01	0.30**	49	0.005	0.29**	36	0.004	0.62	13	High ECa-3m (−)
NH	0.09	0.90**	9	0.07	0.94**	5	0.08	0.95	4	$NH_4^+$$_{5–10cm}$ (+)

** Statistically significant at $p < 0.01$.

† OP, oak–pine; CH, cove hardwood; MO, mixed oak (both low and high elevation); NH, northern hardwood.

‡ ECa-3m-high, highest conductivity value measured; $NH_4^+$$_{5–10cm}$, NH_4^+ concentration at the 5–10-cm depth.
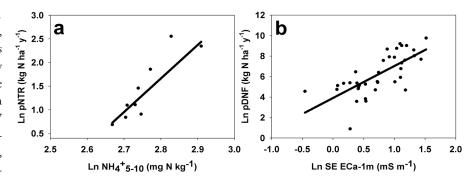

Fig. 4. Potential nitrification rates (pNTR) regressed against (a) the NH_4^+ concentrations at the 5- to 10-cm soil depth in the northern hardwood site ($p < 0.001$, $r^2 = 0.90$) and (b) potential denitrification rates (pDNF) regressed against the standard error of the bulk conductivity (SE ECa-1m) for Watershed 27 ($p < 0.001$, $r^2 = 0.70$).

Table 6. Regression analyses for potential denitrification; + indicates the direction of the relationship; *n* is the total number of values used in the model (four missing samples for SE ECa-1m). The validation statistics are representative of a regression analysis between observed and predicted values.

Site†	Entire data set			Calibration data set			Validation data set			Parameters‡
	RMSE	r^2	n	RMSE	r^2	n	RMSE	r^2	n	
All sites	1.37	0.15 **	75	1.30	0.11*	52	1.47	0.32**	23	C (+)
OP, CH, MO-low	0.97	0.16**	41	0.91	0.13§	29	1.03	0.41*	12	C (+)
OP	0.64	0.41*	12	¶	¶	¶	¶	¶	¶	C (+)
CH	1.06	0.26*	16	¶	¶	¶	¶	¶	¶	C (+)
MO-low	–	–	13	¶	¶	¶	¶	¶	¶	C (+)
NH, MO-high (Watershed 27)	0.98	0.70**	36	0.98	0.64**	25	0.91	0.84**	11	SE ECa-1m (+)

* Statistically significant at $p < 0.05$.

** Statistically significant at $p < 0.01$.

† OP, oak–pine; CH, cove hardwood; MO-low, low-elevation mixed oak; MO-high, high-elevation mixed oak; NH, northern hardwood.

‡ SE ECa-1m, standard error of the values measured; C, C content.

§ Statistically significant at $p < 0.1$.

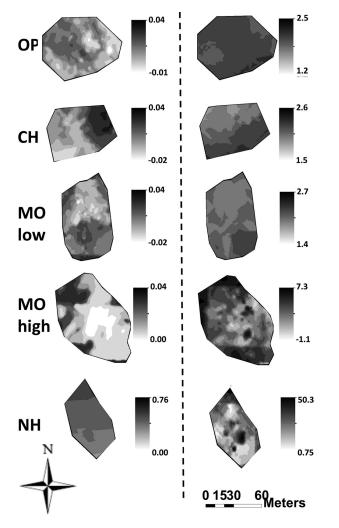¶ Data set was too small to separate into calibration and validation models.

Fig. 5. Predicted potential nitrification (pNTR) (left) and potential denitrification (pDNF) (right) based on electromagnetic induction and near-infrared reflectance spectroscopy data. The numbers represent the natural logarithm of the predicted process rates (μg N kg^{-1} soil d^{-1}) as produced by ordinary kriging. The contour gradient indicates geometric intervals. Potential nitrification was predicted using the highest measured bulk conductivity value at the 3-m depth (ECa-3m-high) for the oak–pine (OP), cove hardwood (CH), low-elevation mesic mixed oak (MO-low) and high-elevation mesic mixed oak (MO-high) sites and NH_4^+ concentrations at the 5- to 10-cm depth for the northern hardwoods site (NH). Potential denitrification was predicted using C (g C m^{-2}) (OP, CH, and MO-low) or the standard error of the bulk conductivity at the 1-m depth (SE ECa-1m) (MO-high and NH).

Conductivity for any given sampling date did not correlate strongly with the abiotic factors assessed (i.e., soil moisture and soil texture); however, the variance in conductivity measurements among dates (SE and ΔECa-3m) and ECa-3m-high were good predictors of abiotic factors. The use of variance measures (i.e., Δ and SE) and maximum values observed (EC-high) is not common but they have proven to be successful variables in more heterogeneous systems (Vachaud et al., 1985; Zhu et al., 2010). Several reasons can be suggested for the value of variance measures. First, soil texture always influences soil conductivity, while soil moisture increases in importance during wetter times. The difference between soil conductivity measured under dry and wet conditions has been demonstrated to be the most effective predictor for hotspots in soil moisture variation in a semiarid rangeland ecosystem (Robinson et al., 2008a). We found a similar result for WS 27, where soil moisture was correlated to SE ECa-1m. Watershed 27 had greater precipitation inputs in combination with finer textured soils that potentially resulted in higher soil moisture retention, as has been found before (Bonito et al., 2003). Alternatively, increases in soil moisture could increase the contribution of soil texture to the overall conductivity signal. In other words, increased soil moisture could act as a conductor and thus allow spatial variance in the soil texture to be more apparent in the soil conductivity measures. For example, Zhu et al. (2010) found soil texture mapping to be most successful with EMI surveys after rain events. Similarly, we found that ECa-3m-high correlated with soil texture only in the wetter WS 27 (Swift et al., 1988), and SE ECa-1m correlated with soil texture in WS 18. Thus, generally, the finer textured and wetter soils in WS 27 resulted in a significant correlation between soil moisture and conductivity (SE ECa-1m) in addition to soil texture and conductivity (ECa-3m-high).

Potential nitrification rates would be expected to be greatest at near-field-capacity soil moisture (Strong et al., 1999), high NH_4^+ availability (Donaldson and Henderson, 1990), high pH (Donaldson and Henderson, 1990; Knoepp and Vose, 2007), low C/N ratios (Knoepp and Vose, 2007), and high O_2 and low CO_2 concentrations (Keeney et al., 1985; Sahrawat, 2008). In forested ecosystems, soil NH_4^+ concentrations are considered the main limiting factor of nitrification rates (Montagnini et al., 1989; Ste-Marie and Paré, 1999), which was the case only for the NH site in this study. For all other sites, an increased ECa-3m-high conductivity, correlated to soil texture, showed a negative relationship with pNTR rates. Higher ECa-3m-high conductivity is related to greater sand content and lower silt content and thus greater gas diffusion rates. Because O_2 availability is one of the main controllers of nitrification (Keeney et al., 1985; Sahrawat, 2008), a higher sand content would allow higher nitrification rates, as was observed by Strong et al. (1999). Alternatively, these results could suggest that the fine particles (i.e., silt and clay) protect NH_4^+ from oxidation and thus reduce the NH_4^+ available for microbial uptake. This was confirmed by Strong et al. (1999) for soils with higher soil moisture content, similar to our NH site, while soils exposed to frequent drying and rewetting events did not show a similar level of physical protection by finer particle sizes.

Overall, pDNF was best predicted by total soil C, as found in previous studies (Groffman and Tiedje, 1991; Luo et al., 1999; Myrold and Tiedje, 1985). However, we found pDNF in WS 27 to be best correlated with conductivity (SE ECa-1m), which probably reflects the strong correlation with soil moisture in WS 27. No improvement in model prediction was accomplished by including total C, and thus C does not appear to be a limiting factor for pDNF in this

Table 7. Semivariogram parameters fitted using a stable fit model with predicted process rates for potential nitrification (pNTR) and potential denitrification (pDNF).

Site†	pNTR				pDNF			
	Major range	Full sill	Nugget	Nugget/sill	Major range	Full sill	Nugget	Nugget/Sill
	m				m			
OP	41	1.1×10^{-5}	0	0	43	0.15	0.11	0.73
CH	>75.4	3.0×10^{-5}	3.4×10^{-6}	0.11	>75.4	0.077	0.058	0.76
MO-low	69	8.8×10^{-6}	0	0	29	0.10	0.031	0.31
MO-high	64	2.1×10^{-5}	2.1×10^{-6}	0.10	0.18	0.015	1.5×10^{-5}	1.0×10^{-3}
NH	>75.4	0.25	0.049	0.20	37	54	0	0

† OP, oak–pine; CH, cove hardwood; MO-low, low-elevation mixed oak; MO-high, high-elevation mixed oak; NH, northern hardwood.

watershed. This is similar to the results of other studies in northern hardwood forests that found that denitrification rates were limited by soil moisture and NO_3^- concentrations rather than organic C due to the high organic C availability at these sites (Groffman, 2012; Groffman and Tiedje, 1988; Melillo et al., 1983).

Plot-scale potential nitrification and potential denitrification rates determined by random sampling compared with EMI and NIRS stratified random sampling showed no significant differences for pNTR in sites with low rates (i.e., OP and MO), whereas rates were greater for CH and NH. Scaling potential denitrification rates to the plot level, however, showed that stratified sampling would result in greater mean rates for all forest types. Stratified sampling generally increased the variability (SE and CV) of the assessment, indicating that the results from random sampling underrepresented hotspot areas in the landscape and thus underestimated overall site N transformation rates. In line with our hypothesis that pNTR would be less heterogeneous than pDNF, the autocorrelation analysis using semivariograms showed a larger range for MO (MO-low and -high) and NH, while showing a similar range for OP and CH. Selecting larger plot sizes might have enhanced the spatial structure and increased model predictive strength in the sites with a larger range than the plot size (pNTR: CH and NH; pDNF: CH).

These data suggest that on the plot scale (ha), assessing heterogeneity is most important in cove and northern hardwood systems, potentially underestimating rates by as much as 200%. The importance of soil heterogeneity has been shown by previous studies for soil nutrient concentrations (Johnson et al., 2010, 2011) and processes (Groffman and Tiedje, 1989; Harms and Grimm, 2008; Vidon et al., 2010), but rarely with the high resolution needed for plot-level assessment. We found no strong significant correlations between pNTR and pDNF. This uncoupled nature could be the result of low C/NH_4^+ ratios in OP, CH, and MO (Chiu et al., 2007), while in NH it could be due to lower O_2 concentrations, as indicated by higher soil moisture (Focht and Verstraete, 1977) and lower sand content (Strong et al., 1999).

This study showed improved precision in extrapolating biogeochemical data to an ecologically relevant scale through the use of geophysical approaches that provide high-resolution spatial data. Including spatially dependent data increases the representative estimates and reduces sampling redundancy for N cycling processes. However, site-specific calibration to the biotic processes of interest is generally required. These approaches will enable us to assess the spatial variability of biogeochemical cycling and improve extrapolation by stratified sampling methods. Combining geophysical and stratified sampling allowed us to address more specific questions regarding the regulation of N cycling processes. Approaches similar to the one utilized in this study are needed across multiple spatial scales to better parameterize the biogeochemical models of the future.

Table 8. Comparison of the effectiveness of extrapolation for potential nitrification (pNTR) and potential denitrification (pDNF) as assessed by random selection and by stratified selection (determined by quartiles) based electromagnetic induction and near-infrared reflectance spectroscopy data (n = 8 for both approaches, except for pNTR 427 and pNTR 527 n = 4).

Site†	pNTR						pDNF					
	Random			Stratified random			Random			Stratified random		
	Rate	SE	CV	Rate	SE	CV	Rate	SE	CV	Rate	SE	CV
	µg N kg⁻¹ soil h⁻¹			µg N kg⁻¹ soil h⁻¹			µg N kg⁻¹ soil h⁻¹			µg N kg⁻¹ soil h⁻¹		
OP	−0.01	0.01	394	0.02	0.03	386	200.7	81.5	115	210.7	81.6	110
CH	0.06	0.03	127	0.07	0.03	117	426.2	114.4	76	1247.7	754.3	171
MO-low	−0.02	0.01	124	0.001	0.01	2169	168.9	34.0	57	193.1	37.6	55
MO-high	−0.02	0.03	225	−0.02	0.03	274	161.4	29.3	51	200.0	34.8	49
NH	2.2	0.6	53	2.9	1.0	66	3874.4	892.5	65	5456.6	1969.8	102

† OP, oak–pine; CH, cove hardwood; MO-low, low-elevation mixed oak; MO-high, high-elevation mixed oak; NH, northern hardwood.

REFERENCES

Abdu, H., D.A. Robinson, M.S. Seyfried, and S. Jones. 2008. Geophysical imaging of watershed subsurface patterns and prediction of soil texture and water holding capacity. Water Resour. Res. 44:W00D18. doi:10.1029/2008WR007043.

Aber, J., W. McDowell, K. Nadelhoffer, A. Magill, G. Berntson, M. Kamakea, et al. 1998. Nitrogen saturation in temperate forest ecosystems. BioScience 48:921–934. doi:10.2307/1313296

Aber, J.D., K.J. Nadelhoffer, P. Steudler, and J.M. Melillo. 1989. Nitrogen saturation in northern forest ecosystems. BioScience 39:378–386. doi:10.2307/1311067

Band, L., C. Tague, P. Groffman, and K. Belt. 2001. Forest ecosystem processes at the watershed scale: Hydrological and ecological controls of nitrogen export. Hydrol. Processes 15:2013–2028. doi:10.1002/hyp.253

Beamish, D. 2011. Low induction number, ground conductivity meters: A correction procedure in the absence of magnetic effects. J. Appl. Geophys. 75:244–253. doi:10.1016/j.jappgeo.2011.07.005

Bendschneider, K., and R.I. Robinson. 1952. A new spectrophotometric method for the determination of nitrite in sea water. J. Mar. Res. 11:87–96.

Bodelier, P.L.E., J.A. Libochant, C. Blom, and H.J. Laanbroek. 1996. Dynamics of nitrification and denitrification in root-oxygenated sediments and adaptation of ammonia-oxidizing bacteria to low-oxygen or anoxic habitats. Appl. Environ. Microbiol. 62:4100–4107.

Bonito, G.M., D.C. Coleman, B.L. Haines, and M.L. Cabrera. 2003. Can nitrogen budgets explain differences in soil nitrogen mineralization rates of forest stands along an elevation gradient? For. Ecol. Manage. 176:563–574. doi:10.1016/S0378-1127(02)00234-7

Breuer, L., R. Kiese, and K. Butterbach-Bahl. 2002. Temperature and moisture effects on nitrification rates in tropical rain-forest soils. Soil Sci. Soc. Am. J. 66:834–844. doi:10.2136/sssaj2002.0834

Burgin, A.J., P.M. Groffman, and D.N. Lewis. 2010. Factors regulating denitrification in a riparian wetland. Soil Sci. Soc. Am. J. 74:1826–1833. doi:10.2136/sssaj2009.0463

Cabrera, M.L. 1993. Modeling the flush of nitrogen mineralization caused by drying and rewetting soils. Soil Sci. Soc. Am. J. 57:63–66. doi:10.2136/sssaj1993.03615995005700010012x

Chang, C.-W., and D.A. Laird. 2002. Near-infrared reflectance spectroscopic analysis of soil C and N. Soil Sci. 167:110–116. doi:10.1097/00010694-200202000-00003

Chiu, Y.-C., L.-L. Lee, C.-N. Chang, and A.C. Chao. 2007. Control of carbon and ammonium ratio for simultaneous nitrification and denitrification in a sequencing batch bioreactor. Int. Biodeterior. Biodegrad. 59:1–7. doi:10.1016/j.ibiod.2006.08.001

Cockx, L., M. Van Meirvenne, and G. Hofman. 2005. Characterization of nitrogen dynamics in a pasture soil by electromagnetic induction. Biol. Fertil. Soils 42:24–30. doi:10.1007/s00374-005-0866-3

Corwin, D.L., and S.M. Lesch. 2005. Apparent soil electrical conductivity measurements in agriculture. Comput. Electron. Agric. 46:11–43. doi:10.1016/j.compag.2004.10.005

Coweeta Long-Term Ecological Research. 1934–2011.1011: Coweeta LTER climate data. [Database.] U.S. For. Serv., Coweeta Hydrol. Lab., Otto, NC. http://coweeta.uga.edu/dbpublic/dataset_details.asp?accession=1011.

Donaldson, J.M., and G.S. Henderson. 1990. Nitrification potential of secondary-succession upland oak forests: I. Mineralization and nitrification during laboratory incubations. Soil Sci. Soc. Am. J. 54:892–897. doi:10.2136/sssaj1990.03615995005400030047x

Doolittle, J.A., K.A. Sudduth, N.R. Kitchen, and S.J. Indorante. 1994. Estimating depths to claypans using electromagnetic induction methods. J. Soil Water Conserv. 49:572–575.

Everett, M.E. 2005. What do electromagnetic induction responses measure? Leading Edge 24:154–157.

Fierer, N., and J.P. Schimel. 2002. Effects of drying–rewetting frequency on soil carbon and nitrogen transformations. Soil Biol. Biochem. 34:777–787. doi:10.1016/S0038-0717(02)00007-X

Firestone, M.K., R.B. Firestone, and J.M. Tiedje. 1980. Nitrous oxide from soil denitrification: Factors controlling its biological production. Science 208:749–751. doi:10.1126/science.208.4445.749

Focht, D.D., and W. Verstraete. 1977. Biochemical ecology of nitrification and denitrification. Adv. Microb. Ecol. 1:135–214.

Friedman, S.P. 2005. Soil properties influencing apparent electrical conductivity: A review. Comput. Electron. Agric. 46:45–70. doi:10.1016/j.compag.2004.11.001

Gragson, T.L., and P.V. Bolstad. 2006. Land use legacies and the future of southern Appalachia. Soc. Nat. Resour. 19:175–190. doi:10.1080/08941920500394857

Groffman, P.M. 2012. Terrestrial denitrification: Challenges and opportunities. Ecol. Processes 1. doi:10.1186/2192-1709-1-11

Groffman, P.M., K. Butterbach-Bahl, R.W. Fulweiler, A.J. Gold, J.L. Morse, E.K. Stander, et al. 2009. Challenges to incorporating spatially and temporally explicit phenomena (hotspots and hot moments) in denitrification models. Biogeochemistry 93:49–77. doi:10.1007/s10533-008-9277-5

Groffman, P.M., E.A. Holland, D.D. Myrold, G.P. Robertson and X. Zou. 1999. Denitrification. In: G.P. Robertson et al., editors, Standard soil methods for long-term ecological research. Oxford Univ. Press, Oxford, UK. p. 272–288.

Groffman, P.M., and J.M. Tiedje. 1988. Denitrification hysteresis during wetting and drying cycles in soil. Soil Sci. Soc. Am. J. 52:1626–1629. doi:10.2136/sssaj1988.03615995005200060022x

Groffman, P.M., and J.M. Tiedje. 1989. Denitrification in north temperate forest soils: Spatial and temporal patterns at the landscape and seasonal scales. Soil Biol. Biochem. 21:613–620. doi:10.1016/0038-0717(89)90053-9

Groffman, P.M., and J.M. Tiedje. 1991. Relationships between denitrification, CO_2, production and air-filled porosity in soils of different texture and drainage. Soil Biol. Biochem. 23:299–302. doi:10.1016/0038-0717(91)90067-T

Groffman, P.M., J.M. Tiedje, G.P. Robertson, and S. Christensen. 1988. Denitrification at different temporal and geographical scales: Proximal and distal controls. In: J.R. Wilson, editor, Advances in nitrogen cycling in agricultural ecosystems. CAB Int., Wallingford, UK. p. 174–192.

Harms, T.K., and N.B. Grimm. 2008. Hot spots and hot moments of carbon and nitrogen dynamics in a semiarid riparian zone. J. Geophys. Res. 113:G101020. doi:10.1029/2007JG000588

Hedley, C.B., I.J. Yule, C.R. Eastwood, T.G. Shepherd, and G. Arnold. 2004. Rapid identification of soil textural and management zones using electromagnetic induction sensing of soils. Aust. J. Soil Res. 42:389–400. doi:10.1071/SR03149

Huth, N., and P. Poulton. 2007. An electromagnetic induction method for monitoring variation in soil moisture in agroforestry systems. Aust. J. Soil Res. 45:63–72. doi:10.1071/SR06093

Isaaks, E.H., and R.M. Srivastava. 1989. Applied geostatistics. Oxford Univ. Press, Oxford, UK.

Janik, L.J., R.H. Merry, and J.O. Skjemstad. 1998. Can mid infrared diffuse reflectance analysis replace soil extractions? Aust. J. Exp. Agric. 38:681–696. doi:10.1071/EA97144

Johnson, D.W., D.W. Glass, J.D. Murphy, C.M. Stein, and W.W. Miller. 2010. Nutrient hot spots in some Sierra Nevada forest soils. Biogeochemistry 101:93–103. doi:10.1007/s10533-010-9423-8

Johnson, D.W., W.W. Miller, B.M. Rau, and M.W. Meadows. 2011. The nature and potential causes of nutrient hotspots in a Sierra Nevada forest soil. Soil Sci. 176:596–610. doi:10.1097/SS.0b013e31823120a2

Johnston, K., J.M. Ver Hoef, K. Krivoruchko, and N. Lucas. 2001. ArcGIS 9: Using ArcGIS Geostatistical Analyst. ESRI, Redlands, CA.

Keeney, D.R., K.L. Sahrawat, and S.S. Adams. 1985. Carbon dioxide concentration in soil: Effects on nitrification, denitrification and associated nitrous oxide production. Soil Biol. Biochem. 17:571–573. doi:10.1016/0038-0717(85)90027-6

Knoepp, J.D., and B.D. Clinton. 2009. Riparian zones in southern Appalachian headwater catchments: Carbon and nitrogen responses to forest cutting. For. Ecol. Manage. 258:2282–2293. doi:10.1016/j.foreco.2009.04.006

Knoepp, J.D., and W.T. Swank. 1998. Rates of nitrogen mineralization across an elevation and vegetation gradient in the southern Appalachians. Plant Soil 204:235–241. doi:10.1023/A:1004375412512

Knoepp, J.D., and J.M. Vose. 2007. Regulation of nitrogen mineralization and nitrification in southern Appalachian ecosystems: Separating the relative importance of biotic vs. abiotic controls. Pedobiologia 51:89–97. doi:10.1016/j.pedobi.2007.02.002

Knoepp, J.D., J.M. Vose, and W.T. Swank. 2008. Nitrogen deposition and cycling across an elevation and vegetation gradient in southern Appalachian forests. Int. J. Environ. Stud. 65:391–410. doi:10.1080/00207230701862348

Luo, J., R.W. Tillman, and P.R. Ball. 1999. Factors regulating denitrification

in a soil under pasture. Soil Biol. Biochem. 31:913–927. doi:10.1016/S0038-0717(99)00013-9

McBride, R.A., S.C. Shrive, and A.M. Gordon. 1990. Estimating forest soil quality from terrain measurements of apparent electrical conductivity. Soil Sci. Soc. Am. J. 54:290–293. doi:10.2136/sssaj1990.03615995005400010047x

McClain, M.E., E.W. Boyer, C.L. Dent, S.E. Gergel, N.B. Grimm, P.M. Groffman, et al. 2003. Biogeochemical hot spots and hot moments at the interface of terrestrial and aquatic ecosystems. Ecosystems 6:301–312. doi:10.1007/s10021-003-0161-9

Melillo, J.M., J.D. Aber, P.A. Steudler, and J.P. Schimel. 1983. Denitrification potentials in a successional sequence of northern hardwood forest stands. Ecol. Bull. 35:217–228.

Montagnini, F., B. Haines, and W. Swank. 1989. Factors controlling nitrification in soils of early successional and oak/hickory forests in the southern Appalachians. For. Ecol. Manage. 26:77–94. doi:10.1016/0378-1127(89)90037-6

Myrold, D.D., and J.M. Tiedje. 1985. Establishment of denitrification capacity in soil: Effects of carbon, nitrate and moisture. Soil Biol. Biochem. 17:819–822. doi:10.1016/0038-0717(85)90140-3

Nielsen, T.H., and N.P. Revsbech. 1998. Nitrification, denitrification, and N-liberation associated with two types of organic hot-spots in soil. Soil Biol. Biochem. 30:611–619. doi:10.1016/S0038-0717(97)00211-3

Parkin, T.B., J.L. Starr, and J.J. Meisinger. 1987. Influence of sample size on measurement of soil denitrification. Soil Sci. Soc. Am. J. 51:1492–1501. doi:10.2136/sssaj1987.03615995005100060017x

Parton, W.J., A.R. Mosier, D.S. Ojima, D.W. Valentine, D.S. Schimel, K. Weier, and A.E. Kulmala. 1996. Generalized model for N_2 and N_2O production from nitrification and denitrification. Global Biogeochem. Cycles 10:401–412. doi:10.1029/96GB01455

Pastor, J., J.D. Aber, C.A. McClaugherty, and J.M. Melillo. 1984. Aboveground production and N and P cycling along a nitrogen mineralization gradient on Blackhawk Island, Wisconsin. Ecology 65:256–268. doi:10.2307/1939478

Pastor, J., and W.M. Post. 1986. Influence of climate, soil moisture, and succession on forest carbon and nitrogen cycles. Biogeochemistry 2:3–27. doi:10.1007/BF02186962

Reedy, R.C., and B.R. Scanlon. 2003. Soil water content monitoring using electromagnetic induction. J. Geotech. Geoenviron. Eng. 129:1028–1039. doi:10.1061/(ASCE)1090-0241(2003)129:11(1028)

Robertson, G.P., D.C. Coleman, C.S. Bledsoe, and P. Sollins. 1999. Standard soil methods for long-term ecological research. Oxford Univ. Press, Oxford, UK.

Robertson, G.P., and P.M. Vitousek. 1981. Nitrification potentials in primary and secondary succession. Ecology 62:376–386. doi:10.2307/1936712

Robinson, D.A., H. Abdu, S.B. Jones, M. Seyfried, I. Lebron, and R. Knight. 2008a. Eco-geophysical imaging of watershed-scale soil patterns links with plant community spatial patterns. Vadose Zone J. 7:1132–1138. doi:10.2136/vzj2008.0101

Robinson, D.A., C.S. Campbell, J.W. Hopmans, B.K. Hornbuckle, S.B. Jones, R. Knight, et al. 2008b. Soil moisture measurement for ecological and hydrological watershed-scale observatories: A review. Vadose Zone J. 7:358–389. doi:10.2136/vzj2007.0143

Sahrawat, K.L. 2008. Factors affecting nitrification in soils. Commun. Soil Sci. Plant Anal. 39:1436–1446. doi:10.1080/00103620802004235

Schimel, J.P., and J. Bennett. 2004. Nitrogen mineralization: Challenges of a changing paradigm. Ecology 85:591–602. doi:10.1890/03-8002

Sheets, K.R., and J.M.H. Hendrickx. 1995. Noninvasive soil water content measurement using electromagnetic induction. Water Resour. Res. 31:2401–2409. doi:10.1029/95WR01949

Sheets, K.R., J.P. Taylor, and J.M.H. Hendrickx. 1994. Rapid salinity mapping by electromagnetic induction for determining riparian restoration potential. Restor. Ecol. 2:242–246. doi:10.1111/j.1526-100X.1994.tb00056.x

Ste-Marie, C., and D. Paré. 1999. Soil, pH and N availability effects on net nitrification in the forest floors of a range of boreal forest stands. Soil Biol. Biochem. 31:1579–1589. doi:10.1016/S0038-0717(99)00086-3

Strong, D.T., P.W.G. Sale, and K.R. Helyar. 1999. The influence of the soil matrix on nitrogen mineralisation and nitrification: IV. Texture. Aust. J. Soil Res. 37:329–344. doi:10.1071/S98043

Swank, W.T., and D.A. Crossley, Jr., editors. 1988. Forest hydrology and ecology at Coweeta. Ecol. Stud. 66. Springer-Verlag, New York.

Swift, J.W., Jr., G.B. Cunningham, and J.E. Douglass. 1988. Climatology and hydrology. Ecol. Stud. 66:35–55.

Tague, C. 2009. Modeling hydrologic controls on denitrification: Sensitivity to parameter uncertainty and landscape representation. Biogeochemistry 93:79–90. doi:10.1007/s10533-008-9276-6

Tague, C., L. Band, S. Kenworthy, and D. Tenebaum. 2010. Plot-and watershed-scale soil moisture variability in a humid Piedmont watershed. Water Resour. Res. 46:W12541. doi:10.1029/2009WR008078

Thomas, D.J. 1996. Soil survey of Macon County, North Carolina. U.S. Gov. Print. Office, Washington, DC.

Tiedje, J.M., A.J. Sexstone, T.B. Parkin, and N.P. Revsbech. 1984. Anaerobic processes in soil. Plant Soil 76:197–212. doi:10.1007/BF02205580

Triantafilis, J., and S.M. Lesch. 2005. Mapping clay content variation using electromagnetic induction techniques. Comput. Electron. Agric. 46:203–237. doi:10.1016/j.compag.2004.11.006

Vachaud, G., A. Passerat de Silans, P. Balabanis, and M. Vauclin. 1985. Temporal stability of spatially measured soil water probability density function. Soil Sci. Soc. Am. J. 49:822–828. doi:10.2136/sssaj1985.03615995004900040006x

van Vuuren, J.A.J., J.H. Meyer, and A.S. Claassens. 2006. Potential use of near infrared reflectance monitoring in precision agriculture. Commun. Soil Sci. Plant Anal. 37:2171–2184. doi:10.1080/00103620600817382

Vidon, P., C. Allan, D. Burns, T.P. Duval, N. Gurwick, S. Inamdar, et al. 2010. Hot spots and hot moments in riparian zones: Potential for improved water quality management. J. Am. Water Resour. Assoc. 46:278–298. doi:10.1111/j.1752-1688.2010.00420.x

Wallenstein, M.D., D.D. Myrold, M. Firestone, and M. Voytek. 2006. Environmental controls on denitrifying communities and denitrification rates: Insights from molecular methods. Ecol. Appl. 16:2143–2152. doi:10.1890/1051-0761(2006)016[2143:ECODCA]2.0.CO;2

Webster, R., and M.A. Oliver. 2005. Modeling spatial variation of soil as random functions. In: S. Grunewald, editor, Environmental soil–landscape modeling: Geographic information technologies and pedometrics. CRC Press, Boca Raton, FL. p. 241–289.

Weller, U., M. Zipprich, M. Sommer, W. Zu Castell, and M. Wehrhan. 2007. Mapping clay content across boundaries at the landscape scale with electromagnetic induction. Soil Sci. Soc. Am. J. 71:1740–1747. doi:10.2136/sssaj2006.0177

Zhang, N., M. Wang, and N. Wang. 2002. Precision agriculture: A worldwide overview. Comput. Electron. Agric. 36:113–132. doi:10.1016/S0168-1699(02)00096-0

Zhu, Q., and H.S. Lin. 2010. Comparing ordinary kriging and regression kriging for soil properties in contrasting landscapes. Pedosphere 20:594–606. doi:10.1016/S1002-0160(10)60049-5

Zhu, Q., H. Lin, and J. Doolittle. 2010. Repeated electromagnetic induction surveys for improved soil mapping in an agricultural landscape. Soil Sci. Soc. Am. J. 74:1763–1774. doi:10.2136/sssaj2010.0056